Materials and Structures (2016) 49:941–960
DOI 10.1617/s11527-015-0550-5

ORIGINAL ARTICLE

Composition, uses, provenance and stability of rocks and ancient mortars in a Theban Tomb in Luxor (Egypt)

S. Cuezva · J. Garcia-Guinea · A. Fernandez-Cortes · D. Benavente · J. Ivars · J. M. Galan · S. Sanchez-Moral

Received: 25 August 2014 / Accepted: 27 January 2015 / Published online: 1 February 2015

Abstract The rock-cut tomb–chapel of Djehuty (Luxor, Egypt, 1470 BC) was excavated and restored including a mineralogical, chemical, textural and petrophysical study of mortars and host rocks together with micro-environmental parameter recordings to deduce the techniques used by the ancient Egyptian builders. The host rock is made by alternations of massive, nodular and finely bedded micritic limestone and the tomb was excavated in the stratigraphic section with better mechanical properties. Different types of gypsum and lime mortars were found in the funerary complex: mortar for bedding, exterior render, surface repair and decoration, and interior plaster and coating. Mortars show formulae according to their specific applications and locations. The sources of the raw materials for the mortar reveal a local provenance. Micro-environmental conditions play an important role in the evolution of the mortar pastes, and determine the current characteristics and stability of mortars. Results from this research will make it possible to design mortars compatible with conservation in the funerary complex of Djehuty and to define safe micro-environmental conditions for the preservation of such mortars and paintings.

Keywords Ancient Egyptian material · Mortar · Micro-environment · Theban tomb · Gypsum · Anhydrite

S. Cuezva · J. Garcia-Guinea (✉) ·
A. Fernandez-Cortes · S. Sanchez-Moral
Museo Nacional de Ciencias Naturales (CSIC), C/Jose Gutiérrez Abascal 2, 28006 Madrid, Spain
e-mail: guinea@mncn.csic.es

D. Benavente
Departamento Ciencias de la Tierra y del Medio Ambiente Unidad Asociada UA-CSIC, Universidad de Alicante, 03080 Alicante, Spain

J. Ivars · J. M. Galan
Centro de Ciencias Humanas y Sociales (CSIC), C/Albasanz 26-28, 28037 Madrid, Spain

1 Introduction

The degradation of building materials of architectural heritage is of great interest among scientists since new restoration materials frequently fail to guarantee compatibility with the ancient masonry and weathered surfaces [1, 2]. Research into composition, physical properties, uses, production and provenance of ancient construction materials including rocks substrata is of great significance for achieving the future effective conservation of ancient monuments [3, and citations therein]. Moreover, the study of microclimate conditions and environmental monitoring has emerged as an essential research for the conservation and restoration of monuments [4]. The restricted published studies on Egyptian stones, mortars, plasters and stuccoes, i.e., ancient-originals, historical-restorations and suitable restoration mortars, provide crucial information for conserving this valuable cultural heritage and the future wealth of the associated tourist activity. The publications to date are concerning the porous structure and composition of mortars [5–9], the geomechanics of stones and mortars [10–12] and soluble salts deteriorating Pharaonic and Coptic wall paintings [13, 14]. Besides, the long-term monitoring of the microclimatic and environmental factors of the sites has proved that these are one of the key issues addressing the preservation and management of these ancient Egyptian monuments, particularly for evaluating and managing the effects of visitors on the conditions of the tombs [15].

The complete characterization of the physical–mechanical, microstructural and chemical properties of both host rock and ancient mortars is crucial for choosing suitable repair mortars so as to preserve the integrity and authenticity of ancient structures [16, 17]. In this regard, RILEM (The International Union of Laboratories and Experts in Construction Materials, Systems and Structures) publications provide useful recommendations for classifying the functions and nature of binder and aggregate in mortars and on the most appropriate methods and techniques for studying them [18–20]. For the preparation of ancient mortars and concretes, various materials were employed such as gypsum limes used for rendering, but carbonated limes were predominantly used in structural mortars [21].

The study of rock and mortars started in 2002 within a long-term Spanish archaeological mission working on the West Bank of Luxor to excavate and restore the rock-cut tomb–chapel of Djehuty (TT 11) at the foothill slope of Dra Abu el-Naga, ca. 1470 BC [22, 23]. The tomb–chapel was decorated in relief and hewn out of a carbonate sedimentary sequence with diverse properties belonging to the well-known Thebes geological formation [24, 25]. The complex monument contains different types of mortars used according to different building functions. The aim of this paper is to characterize host rocks of the tomb–chapel together with ancient Egyptian mortars classifying their functions and nature of binder and aggregates following the RILEM recommendations [18–20]. Nearly fifty micro-samples of mortars and rocks were analysed by environmental scanning electron microscopy (ESEM) with an attached X-ray energy dispersive system (EDS) and spectral cathodoluminescence detector (CL), X-ray diffraction (XRD), X-ray spectrometry analysis (XRF) and mercury intrusion porosimetry (MIP). The external meteorological conditions of the archaeological site and the micro-environment conditions inside Djehuty's tomb–chapel were simultaneously recorded.

2 Site, materials and methods

2.1 The rock-cut tomb–chapel of Djehuty (TT11)

The rock-cut tomb–chapel of Djehuty (TT 11) under study is dated to the early eighteenth Dynasty, ca. 1470 BC [22]. It is located in the central area of Dra Abu el-Naga, at the northern end of the Theban necropolis (Luxor, Egypt) (Fig. 1). The monument has an *open courtyard* 34 m long and a width that varies between 7.60 m (tomb–chapel façade) to 6.30 m (court entrance) (Figs. 1, 2). The side walls are carved in rock, being extended by a mud–brick (adobe) wall on the West side and by masonry surmounted by layers of mud–bricks on the East wall, reaching a height of at least 2.91 m. There are remains of the mortar that covered the side walls, both on the hill rock and on the mud–bricks. The tomb of Djehuty originally had an *open*, *roofless hall* (closed and covered by the Department of Antiquities of Egypt since the 1960s), with inscriptions on both sides of the original door of the tomb and sculpture of Djehuty which are carved on its North and East walls respectively. The *sculpture of Djehuty* was set into a white niche of hard lime mortar. The tomb–chapel mainly consists of two levels. The upper level of the tomb–chapel, the *funerary chapel*, is in the shape of an inverted T. The inner part penetrates horizontally 18 m inside the rock of the hill. First a *transverse corridor* has relief decoration showing a variety of different scenes and inscriptions carved on its walls. Then a narrow *central corridor* leading to the innermost room of the tomb–chapel is also decorated with reliefs. The *innermost room* (*shrine*) is decorated in high quality raised relief displaying the most significant moments of Djehuty's ideal funerary rituals. The right side is entirely occupied by a *funerary shaft* which descends vertically 8.15 m to a broad chamber. At the rear end there is a second shaft, 3 m deep. At the southern shorter side there is an entrance to a second chamber measuring 3.65 m × 3.50 m × 1.55 m. This is the *burial chamber* where the west and north walls and also an area of the ceiling remained coated with mortars

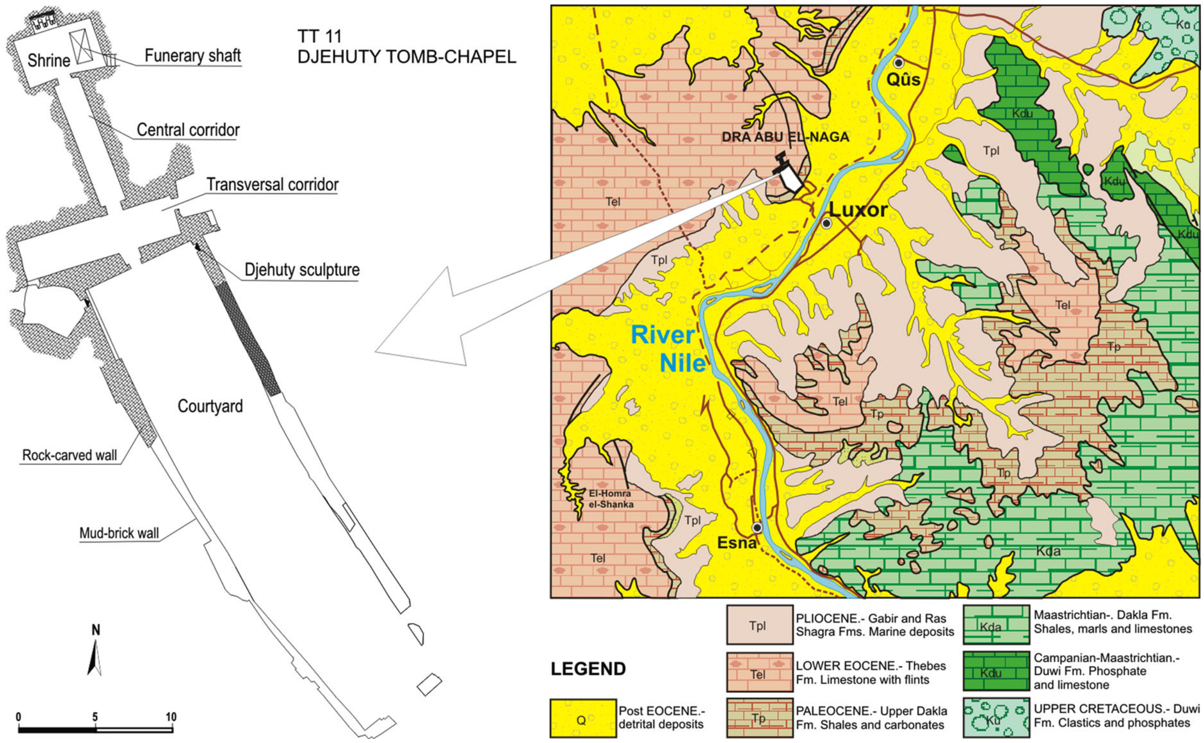

Fig. 1 TT11 Djehuty Tomb–chapel in Luxor (Egypt): geological map of the surrounding area and horizontal sketch

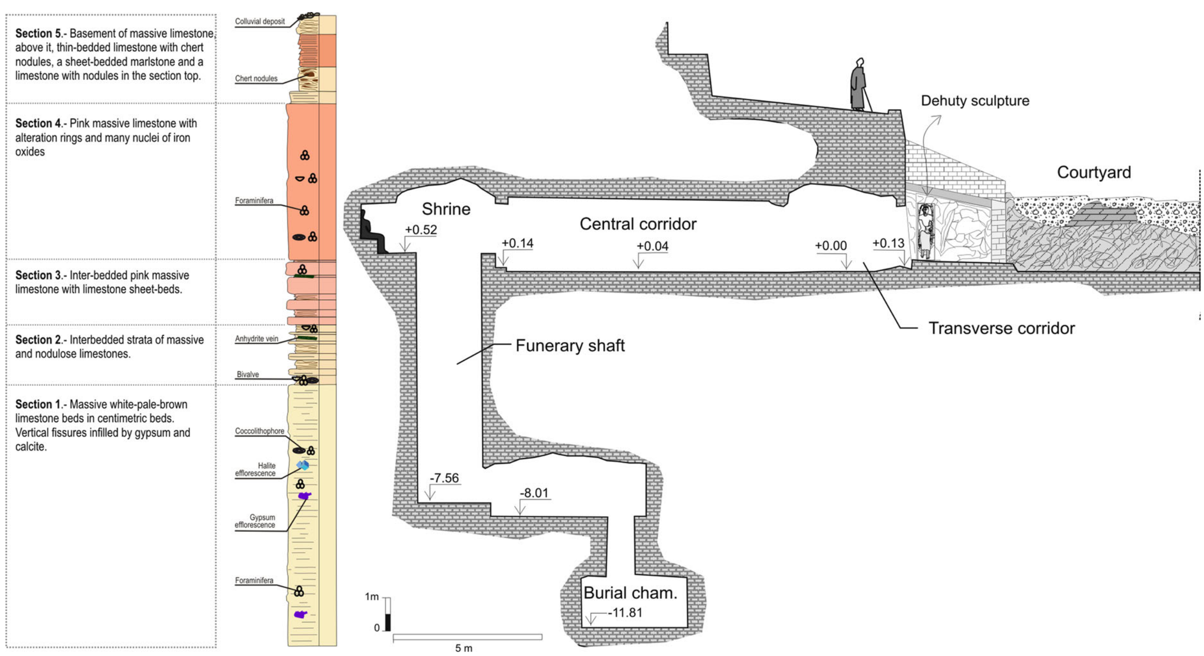

Fig. 2 Vertical sketch section of Djehuty's tomb–chapel including stratigraphic location of its five geological column sections and the lithological and paleontological description

on which passages from one of the earliest Book of the Dead are written [23].

2.2 Geological frame of the rock-cut tomb–chapel of Djehuty (TT11)

The tomb–chapel was hewn into a carbonated sedimentary sequence of Eocene age (Ypresian, 55.8–48.6 million of years), in particular in the lower member (Member I) of the Thebes Formation (Fig. 1). The type-section of this Formation is located at Gebel El-Qurn [24] next to the tombs area, and the stratigraphic sequence was described in detail by Tawfik et al. [25]. Moreover, this geological formation has been extensively studied for its archaeological significance, mainly in the Valley of Kings, e.g., [26, 27]. The local stratigraphic sequence consists of circa 38 m of beds of variable thickness from a few centimetres to several metres mainly composed of massive or nodular limestone rocks. A subdivision into five sub-beds or sections based on field observations was performed and sampled (Fig. 2).

2.3 Climatic and microenvironment monitoring

A monitoring programme was launched in 2008 and it is still working at the archaeological site. Three HOBO-Pro-v2 data-loggers (Onset Computer Corporation, Bourne, USA) with built-in temperature (accuracy ± 0.2 over 0–50 °C, resolution 0.02 at 25 °C) and relative humidity RH (range 0–100 %, accuracy ± 2.5 % from 10 to 90 %, resolution 0.03 %) sensors were installed to record these air parameters on the hour, at three locations: (i) exterior (courtyard), (ii) shrine and (iii) burial chamber.

Also meteorological data of the study area were analysed by using the surface weather conditions of Luxor city for the last 30 years (NOAA's data) [28]. The USAF Luxor station number 624050 (25°40′1.2″N, 32°42′00″W, 87 m.a.s.l) is located in Luxor airport 10.5 km away from Djehuty's tomb–chapel (25°44′11.07″N, 32°37′24.61″E, 101 m.a.s.l).

2.4 Collection of micro-samples and analytical methods

Prior to the micro-invasive sampling, detailed and comprehensive in situ visual analyses were performed together with the necessary understanding of the complexity of the monument, as RILEM indicates [19].

A total of 36 mortar micro-samples were carefully collected from 2006 to 2010 to be analysed by XRD, XRF, ESEM-EDS, CL and MIP depending on the specific minimum sample size. The main sampling criteria for the mortars were the uses or functions in accordance with the RILEM association classifications [18–20]. Samplings were performed by setting the mortar location (i.e. outside, inside, distance to the water table) and mortar colours and textures (Table 1). A second samples collection target was the local geological stratigraphic column to obtain correlation materials to be compared with local mortars for provenance studies (Fig. 2).

Qualitative, quantitative and micro-textural XRD analyses of powdered Egyptian mortar and rock samples were performed using XPOWDER software which allows a full duplex control of the Philips PW-1710/00 diffractometer using the CuKα radiation from 5° to 65° 2θ with a Ni filter and a setting of 40 kV and 40 mA. The chemical XRF analyses were performed in a Magic Philips X-ray fluorescence spectrometer operating an ultra-thin window and rhodium anode X-ray tube at 2.4 kW. The quantitative determinations were performed by both the IQ+ software of Panalytical-Philips and by calibration curve with mineral standards. The environmental electron microscopy studies were performed under a FEI Inspect ESEM microscope. The ESEM resolution at low-vacuum recording the backscattering images was at 4.0 nm at 30 kV Spot samples of EDS analyses and mapping areas were carried out with an energy dispersive X-ray spectrometer, Oxford Instruments INCA Energy 200 Energy Dispersive System. The ESEM microscope has a coupled MONOCL3 Gatan probe to allow the cathodoluminescence spectra recording. Connected porosity and pore size distribution were obtained from MIP with an Autopore IV 9500 Micrometrics mercury porosimeter. The pore size interval characterization by MIP ranged in a radius range of 0.003–200 µm which corresponds respectively to highest and lowest head pressures. The determination of the specific surface area (SSA) was carried out through the BET method in the relative pressure interval $P/P_0 = 0.05$–0.2 using an Autosorb-6 Quantachrome apparatus. Micro-compression characterization was performed in samples sized 10 mm × 10 mm × 10 mm using a uniaxial compression press (Instron 4411) with a maximum load of 5,000 kN and a constant load

Table 1 Setting, use, colour, texture, and RILEM functional classifications of collected samples

Mortar type	Sample	Setting	Building element	Technical application	Mortar color	Mortar texture	RILEM functional mortar classifications	
							RILEM TC 203-RMH [24]	RILEM Workshop 1988 [22]
Bedding mortar	M4	Open courtyard: west wall	Mud–brick masonry wall	Setting and adhesion	Beige	Intermediate–coarse	Bedding mortar	Masonry mortars: (i) bedding
	M21	Open courtyard: west wall	Mud–brick masonry wall	Setting and adhesion	Beige	Coarse	Bedding mortar	Masonry mortars: (i) bedding
	M35–M41	Open courtyard: west wall	Mud–brick masonry wall	Setting and adhesion	Grey–cream	Intermediate	Bedding mortar	Masonry mortars: (i) bedding
	M43–M44	Open courtyard: west wall	Mud–brick masonry wall	Setting and adhesion	Grey–cream	Intermediate	Bedding mortar	Masonry mortars: (i) bedding
	M45–M46	Open courtyard: west wall	Mud–brick masonry wall	Setting and adhesion	Grey–cream	Intermediate–coarse	Bedding mortar	Masonry mortars: (i) bedding
	M49–M50	Open courtyard: west wall	Mud–brick masonry wall	Setting and adhesion	Grey–cream	Intermediate–coarse	Bedding mortar	Masonry mortars: (i) bedding
	M52	Open courtyard: west wall	Mud–brick masonry wall	Setting and adhesion	Grey–cream	Intermediate–coarse	Bedding mortar	Masonry mortars: (i) bedding
Exterior render	M2	Open courtyard: west wall	Rock carved/masonry wall	First mortar-coating layer, for flattening	Brown dark	Coarse	Exterior render	Mortars for the application of facings: (ii) walls
	M16	Open courtyard: east wall	Rock masonry wall	First mortar-coating layer, for flattening	Brown dark	Coarse	Exterior render	Mortars for the application of facings: (ii) walls
	M3	Open courtyard: west wall	Rock carved/masonry wall	Second mortar-coating layer, for smoothing	Brown pale	Intermediate	Exterior render	Mortars for the application of facings: (ii) walls
	M12	Open courtyard: west wall	Mud–brick masonry wall	Single mortar-coating layer, for smoothing	Brown pale	Intermediate	Exterior render	Mortars for the application of facings: (ii) walls
	M13	Open courtyard: west wall	Mud–brick masonry wall	Second mortar-coating layer, for smoothing	Brown pale	Intermediate	Exterior render	Mortars for the application of facings: (ii) walls
	M14	Open courtyard: east wall	Rock masonry wall	Second mortar-coating layer, for smoothing	Brown pale	Intermediate	Exterior render	Mortars for the application of facings: (ii) walls
	M15	Open courtyard: east wall	Rock masonry wall	Second mortar-coating layer, for smoothing	Brown pale	Intermediate	Exterior render	Mortars for the application of facings: (ii) walls
	M20	Open courtyard: west wall	Rock carved/masonry wall	Second mortar-coating layer, for smoothing	Brown pale	Intermediate	Exterior render	Mortars for the application of facings: (ii) walls
	M8	Open courtyard: western wall	Rock carved/masonry wall	Aesthetic layer	White	Fine	Exterior render	Mortars for decoration: (i) layered
	M8-07	Open courtyard: western wall	Mud–brick masonry wall	Aesthetic layer	White	Fine	Exterior render	Mortars for decoration: (i) layered
	M88-08	Open courtyard: western wall	Mud–brick masonry wall	Aesthetic layer	White	Fine	Exterior render	Mortars for decoration: (i) layered
	M9	North façade wall	Rock masonry wall	Aesthetic layer	Grey/white	Fine	Exterior render	Mortars for decoration: (i) layered

Table 1 continued

Mortar type	Sample	Setting	Building element	Technical application	Mortar color	Mortar texture	RILEM functional mortar classifications	
							RILEM TC 203-RMH [24]	RILEM Workshop 1988 [22]
	M10	North façade wall	Rock masonry wall	Aesthetic layer	Grey/white	Fine	Exterior render	Mortars for decoration: (i) layered
	M11	North façade wall	Rock masonry wall	Aesthetic layer	Grey/white	Fine	Exterior render	Mortars for decoration: (i) layered
	M22	Open courtyard: UE-17 well	Mud–brick masonry wall	Aesthetic layer	White	Fine	Exterior render	Mortars for decoration: (i) layered
Surface repair	M5	Open courtyard: west façade	Rock carved wall	Rock fallen replacement/gap filling	White	Fine–intermediate	Mortars for surface repairs	Special mortars for repairs
	M6	Open courtyard: west façade	Rock carved wall	Rock fallen replacement/gap filling	White	Fine–intermediate	Mortars for surface repairs	Special mortars for repairs
	M23	Open courtyard hall	Djehuty sculpture	Replacement and decoration	Grey/white	Fine	Mortars for surface repairs	Special mortars for repairs
	M1	Transverse corridor. SE wall	Rock carved wall	Rock fallen replacement/gap filling	White	Fine–intermediate	Mortars for surface repairs	Special mortars for repairs
	M7	Transverse corridor. NE wall	Rock carved wall	Rock fallen replacement/gap filling	White	Coarse	Mortars for surface repairs	Special mortars for repairs
	M28	Central corridor. west wall	Rock carved wall	Replacement and rock fallen clamping	Grey/white	Intermediate–coarse	Mortars for surface repairs	Special mortars for repairs
	M25	Shrine: west wall	Rock carved wall	Replacement and rock fallen clamping	Grey/white	Coarse	Mortars for surface repairs	Special mortars for repairs
	M26	Shrine: west wall	Rock carved wall	Replacement and decoration	White	Fine	Mortars for surface repairs	Special mortars for repairs
	M27	Shrine: west wall	Rock carved wall	Replacement and rock fallen clamping	Grey/white	Coarse	Mortars for surface repairs	Special mortars for repairs
Interior plasters and coatings	M29	Burial chamber	Rock carved ceiling	First mortar-coating, to flatten and leveling	Grey/white	Intermediate	Interior plaster	1. Mortar for plaster
	M30	Burial chamber	Rock carved ceiling	Aesthetic layer	Grey/white	Fine	Interior plaster	1. Mortar for plaster
	M31	Burial chamber	Rock carved wall	Aesthetic layer	Grey–cream	Intermediate	Interior plaster	1. Mortar for plaster
Mortar for decoration	M24	Open courtyard hall	Djehuty sculpture	Sculpture coatings	White	Fine	–	3. Mortars for decoration: (i) layered

velocity of 0.1 MPa/s. The specimen size was consistent with the standard mechanical tests, which recommend that specimen size should be at least ten times larger than grain size [10].

3 Results

3.1 Climatic and microenvironment conditions

The Luxor climate is severely arid and is classified as hyper-desert and extreme Mediterranean type. During the last 30 years the annual mean temperature of the air was 25.1 °C, with a maximum inter-annual variation below 1.6 °C. The absolute air temperature for each annual cycle has always been ranging from 1.4 to 45 °C on average. Rainfall has been almost anecdotal in the last three decades, and a mere total amount of 470 mm has been registered since 1980 with 43 % of years having a total absence of rainfall events. The rain episodes are centered in few days (3 per year on average) and some of them correspond to torrential events. The dry conditions and extreme temperatures determine a very low RH of air (37.8 % on average) ranging from 32.5 to 40.3 % in terms of annual average.

The environmental monitoring (2008–2011 period) provided measurements on temperature and RH of outdoor air (open courtyard), being warmer and drier (31.5 °C and ~19.5 %, respectively, on annual average) than those registered in Luxor city. Moreover, these extreme environmental conditions are tempered by the neighbouring Nile riverbed. The annual mean temperature of air in Djehuty's innermost room (shrine) drops to 29.5 °C and RH goes up to 22.1 %. When the funerary shaft, 8.20 m deep, was excavated (February 2008), the antechamber was reached and opened. The air temperature and RH remained around 28 °C and slightly above 80 %, respectively. These environmental ranges could be close to those under pristine conditions before any modern archaeological excavation. Similar environmental conditions were registered later at the bottom of another funerary shaft excavated during 2010 (28.5 °C and 78.2 %), which reaches a depth similar to that of the burial chamber of Djehuty. The higher values of RH with depth are related to the proximity of the Nile water table, located from 2.5 to 2 m below the burial chamber.

3.2 Mineralogical, chemical and petrophysical characteristics of host rock

The host rock in which the rock-cut tomb is located consists of alternations of massive, nodular and thinly bedded micritic limestone. The tomb was excavated into four of the five local stratigraphic sections according to field observations (Fig. 2). These sections are described below, with special attention to their mineralogical, chemical and petrophysical characteristics (Figs. 3, 4).

Section 1 (S1) is composed of massive white–pale-brown limestone beds with thicknesses of a few centimetres (Fig. 2). It is the section in which the burial chamber of the tomb was excavated. This limestone is fine grained and quite porous being predominantly composed of the remains of calcareous nano-plankton (mainly coccolithophores, Fig. 5a) and micro-plankton (mainly foraminifers) with abundant fragments of mollusc shells. It shows vertical fissures filled with gypsum and calcite. The XRD analysis (Table 2) shows a predominantly calcite mineral composition (85–90 %). The XRF analyses display a chemical composition in good agreement with the mineralogical composition, with only one sample being observed to have an important amount of Th, Ba and Cl elements and another with some Cs.

Section 2 (S2) exhibits white–pale-brown massive limestone inter-bedded with limestone sheet-beds. Near to the section top, the bed thickness of nodule limestone increases in comparison with massive beds (Fig. 2). The XRD analysis shows a less predominant presence of calcite (75–80 %) (Table 2). The XRF

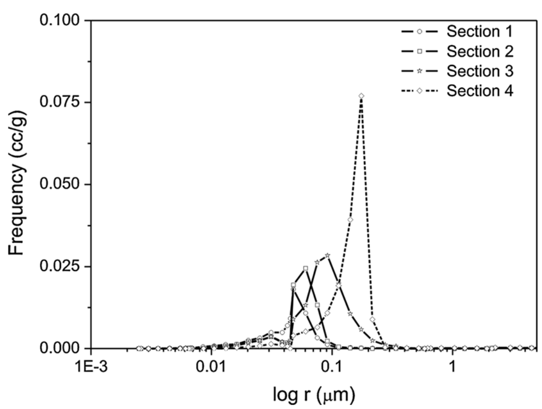

Fig. 3 Pore-size distribution curves of host rocks for the different geological sections

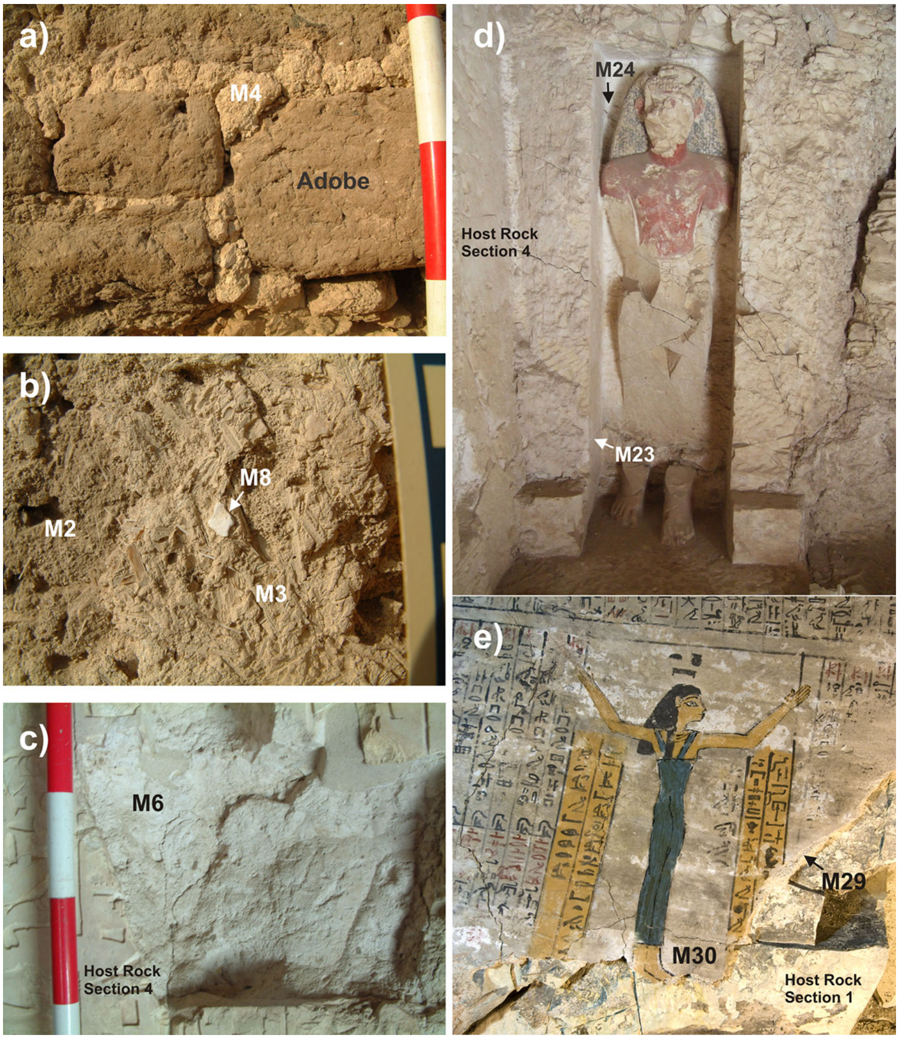

Fig. 4 Photographs of the different types of mortar on the funerary complex of Djehuty: **a** bedding mortar (M4) for setting masonry units (mud–bricks), **b** exterior render mortars showing the first mortar-coating layer (*M*2), the second mortar coating-layer (*M*3) and the final aesthetic layer (*M*8), **c** surface repair mortar (*M*6) used for the replacement of a block of fallen rock during the carving of the tomb–chapel. **d** Djehuty sculpture carved directly in the host-rock (*S*4). The recess on the wall for holding the sculpture is covered by a hard mortar (*M*23) including huntite as bleaching agent on the outer surface (*M*24). **e** Nut represented in the centre of the ceiling of the painted burial chamber. A leveller layer of mortar is applied directly on the lowered and smoothen ceiling (*M*29). This layer is covered by a final plaster layer (*M*30)

analyses display a chemical composition with more Fe, Mg, Cr and Ce.

Section 3 (S3) is composed of inter-bedded strata of pink to white–pale-brown massive and nodule limestone with slightly dolomitized levels. Near the section top, the thickness of the massive beds increases in comparison with the nodule limestone beds (Fig. 2). Section 3 shows the higher proportion of phyllosilicate minerals (Table 2). The XRF analyses display a chemical composition with more Fe, Al, Mg, Sr and Mn. Some higher amounts of S, Cs, Th, Cr, Ba and Ce are is also noticeable.

Section 4 (S4) in which the upper level of the tomb–chapel is located, is pink massive limestone (Fig. 2). The mineral composition is again predominantly calcite (Table 2). The XRF analyses display a chemical composition in agreement with the mineralogical composition.

Petrophysical properties of the host rocks are strongly influenced by their mineralogical and textural

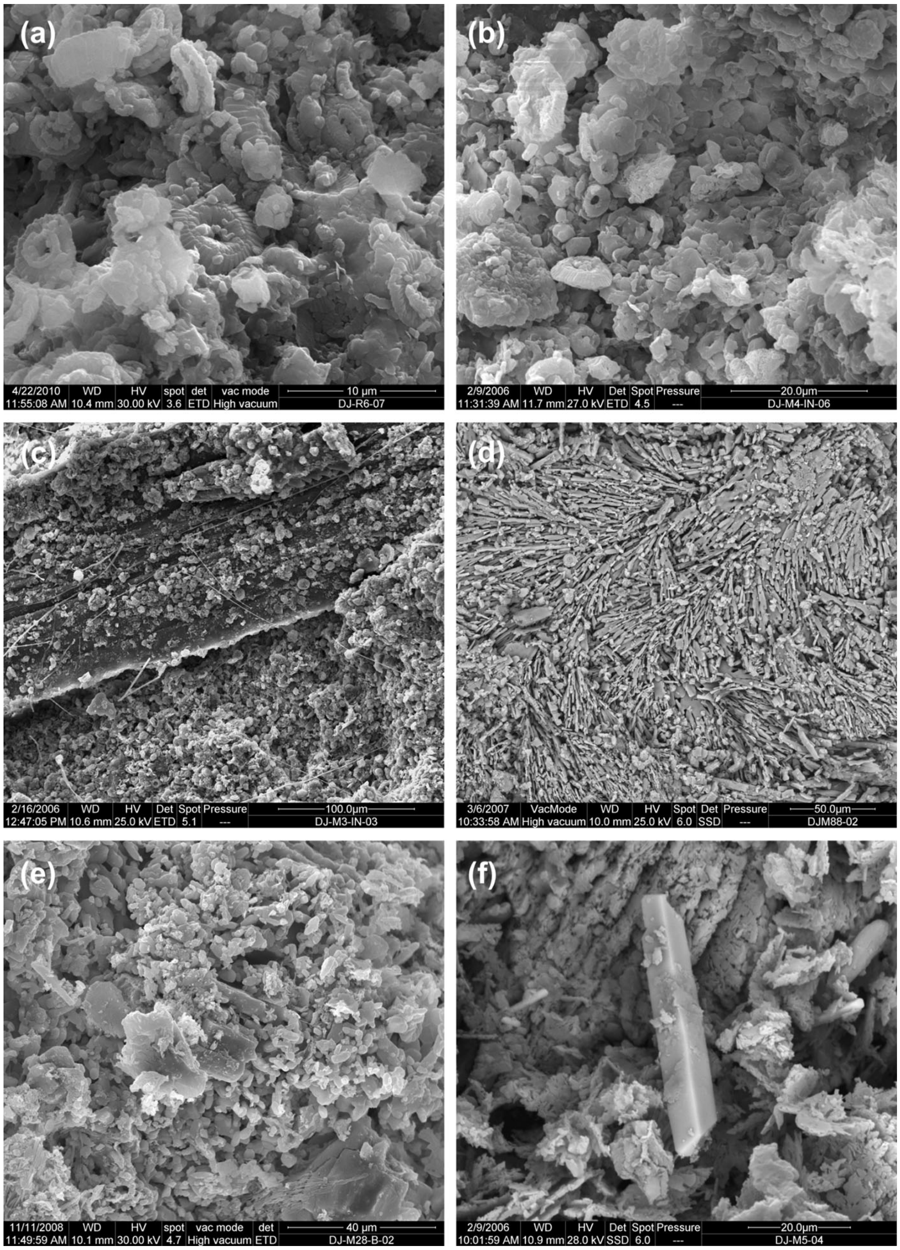

Fig. 5 Photomicrographs taken under the ESEM: **a** calcite fragment from the S4 of the geological column exhibiting coccolithophores; **b** carbonatic bedding mortar sample (M4) including fragments of coccolithophores; **c** carbonatic exterior render (M3) exhibiting straw and Coccolithus fragments; **d** calcium sulphate exterior render mortar sample (M88-7) consisting of anhydrite binder; **e** surface repair mortar sample (M28) composed of anhydrite as binder and detrital quartz and feldspar grains; **f** surface repair mortar sample (M5) with a celestine crystal in detail

characteristics (Table 2). Porosity is mainly inter-particle, increasing from the geological rock cementation decrease from S1 to S4. Porosity values are therefore lower at the bottom of the geological column (S1–S2) than at the top (S3–S4). Some thin fissures and veins are also found randomly distributed. Pore size distribution of the inter-particle porosity highlights the lithological variation through the geological column (Fig. 3). In S1, the host rock is more fine-grained and tends to be less cemented at the top,

Table 2 Value averages of the main physical, chemical and mineralogical properties by sections of the geological column

		Section 1	Section 2	Section 3	Section 4
Mineralogical composition (%)	Calcite	85–90	75–80	65–70	85–90
	Dolomite	1–5	5–10	15–20	1–5
	Quartz	1–5	5–10	5–10	5–10
	Phyllosilicates (mainly illite)	1–5	<1	5–10	–
Chemical composition, minor elements (%)	SiO_2	9.06	11.40	12.74	11.26
	Al_2O_3	2.63	2.01	2.78	1.09
	Fe_2O_3 (total)	0.96	1.23	1.39	0.82
	MnO	0.01	0.01	0.01	0.01
	MgO	1.39	1.84	2.37	1.36
	CaO	44.91	43.30	42.75	44.98
	Na_2O	0.54	0.59	0.59	0.48
	SO_3	0.19	0.32	0.41	0.27
	K_2O	0.36	0.40	0.39	0.13
	TiO_2	0.08	0.09	0.08	0.03
	P_2O_5	0.57	0.75	0.68	0.31
	LOI	39.22	38.00	35.50	39.13
Pore structure properties	Total porosity (He) (%)	18.90	20.40	29.48	33.35
	Connected porosity (Hg) (%)	16.90	17.59	25.95	30.26
	Mean radius (Hg) (μm)	0.057	0.063	0.094	0.157
	Specific surface area, SSA (N_2) (m^2/g)	6.02	3.44	5.72	3.28
Mechanical properties	Compressive strength (MPa)	17.20	26.63	13.82	30.51

meaning the pore size increases from the S1 to S4. The peak height also rises since it reflects the increase in the pore volume or porosity value (Table 2). The pore size displays two pore modes. The most important and abundant has higher values, being related to the intergranular porosity–pore space between bioclasts and/or terrigenous grains. The second pore family presents less pore volume; it is placed at lower pore size values and is formed by micritic calcite and/or clay minerals.

Clay minerals have special importance in both the specific surface area (SSA) and mechanical strength. Host rock in geological S1 and S3 contains phyllosilicates (mainly illite) and also comprises the largest SSA values and lowest compressive strength values (Table 2). The presence of clay minerals increases the surface area of host rock since both are of small size (external surface area related to large area/volume ratio) and micro-porosity (inner surface area), which explains SSA values slightly higher in S1 and S3 than in S2 and S4. The inter-particle clay minerals are usually found in the rock cement, binding the grains together. This type of binding phase reduces the mechanical strength and also increases their likelihood of deteriorating. So the presence of clay minerals produces rock softening [29] and clay-bearing host rock presents less values of compressive strength (S1 and S3). The studied rocks presented a low compressive strength (13–31 MPa). Micro-characterization provides mechanical values in the same range as meso-characterisation of similar kinds of rocks [30]. Moreover, the stress–strain analyses performed in some micro host rocks samples reveal relatively linear stress–strain behaviour and brittle fracture [10].

3.3 Types of mortar on the funerary complex of Djehuty by visual analysis

The in situ visual analysis of the monument allowed us to recognize the main building elements and to distinguish different types of mortar according to their specific applications [19] (Table 1).

(1) *Bedding mortar* or mortar joint is a mortar *for setting* masonry *units* (mud–bricks), *for adhesion and bearing load*, according to the functional categories defined by the RILEM [20]. It

corresponds to the type 4, *Masonry mortars*: (i) *bedding*, defined in the previous RILEM classification [18]. It is located outside the tomb–chapel, and it was used to bind mud–brick and rock units of the open courtyard masonry walls (Fig. 4a). A total of 15 micro-samples collected at different locations were studied.

(2) *Mortar for exterior render* The exterior render group comprises mortar coatings and stuccoes applied to the external surfaces (Fig. 4b), for *water penetration protection and aesthetic covering* [20]. It is layer structured as follows: a first mortar-coating layer, for flattening the rock/mud–brick substrate, when required; a second mortar-coating layer, for smoothing; and lastly an aesthetic layer of stucco. In some cases, only the second layer is present. This mortar corresponds to the type 2, *Mortars for the application of facings:* (ii) *walls* of the previous RILEM classification [18]. It is located outside the tomb–chapel, covering open courtyard masonry (mud–brick and stone blocks) and rock-carved walls. A total of 15 such micro-samples type collected at different locations were studied.

(3) *Mortar for surface repair* is the mortar employed to *replace and repair missing sections of masonry* [20]. It corresponds to the type 5(v) *Special mortars for repairs*, defined in the previous RILEM classification [18]. It is a mortar for clamping and replacing fallen rock. It is used for the replacement of rock fall during the excavation of the tomb and the filling of gaps (Fig. 4c, d, sample M23). It is applied in direct contact with the rock and sometimes includes rock fragments. It is located both inside and outside of the tomb–chapel. A total of nine micro-samples was studied, three located outside and six located inside the tomb–chapel.

(4) *Interior plaster and coating* is an *aesthetic covering*, *a substrate for decoration* [20], employed inside. It is equivalent to the 1, *Mortar for plaster*, defined in the previous RILEM classification of mortars [18]. It is located inside the tomb–chapel, in the burial chamber, and it is applied to walls and ceiling (Fig. 4e). It is layer structured as follows: first, a levelling layer of mortar is applied directly onto the lowered and smooth rock wall/ceiling. This layer is covered by a plaster layer, eventually painted. three micro-samples were studied.

(5) *Mortar for decoration* This type was not included in the last RILEM classification [20], but corresponds to the 3. *Mortars for decoration*: (i) *layered*, (ii) *relief*, defined in the previous RILEM classification [18]. In this group we include the thin mortar layer surrounding the statue of Djehuty, located in the Hall of the Open Courtyard (Fig. 4d).

3.4 Mineralogical, chemical, textural and petrophysical characteristics of mortars

The mineralogical, chemical, textural and petrophysical characteristics of the studied mortars have shown variability mainly related to their specific use and location.

Bedding mortars exhibit variable mineral compositions, with a predominance of calcite as a main mineral component in most samples (Table 3). Average values for these *carbonated bedding mortars* are calcite 56 %, quartz 17 %, illite 10 %, feldspar 7 %, dolomite 4 % anhydrite 3 % gypsum 1 % and sepiolite 1 %. Also there is a second type of bedding mortars, whose main component is calcium sulphate (anhydrite) that appears as another constructive phase. Average values for these calcium *sulphate bedding mortars*: anhydrite 45 %, calcite 32 %, quartz 9 %, illite 4 %, sepiolite 4 %, feldspar 3 % and dolomite 3 %. A third type of bedding mortars whose main component is carbonated mud, appears represented by two samples. The average mineralogical composition of these *carbonated mud bedding mortars* is calcite 25 %, quartz 23 %, illite 17 %, feldspar 14 %, dolomite 2 % and sepiolite 18 %.

Mortars for exterior render exhibit variable mineral compositions related to their structural position (Table 3). The first mortar-coating layer (*carbonate–mud render*), in direct contact with the host rock or mud–bricks, is a mixture of limestone and straw fragments with an average mineral composition of calcite 43 %, quartz 20 %, illite19 %, feldspar 12 %, sepiolite 5 % and dolomite 2 %. The second mortar-coating layer (*carbonated render*), more fine-grained, is mainly composed of a 85–95 % of calcite with minor amounts of quartz and dolomite (3.4 and 2 % average values respectively) and occasionally

Table 3 Mineralogical semi-quantitative DRX analyses of mortars

Mortar type	Sample	Gypsum	Anhydrite	Calcite	Illite	Quartz	Feldspar	Sepiolite	Dolomite
Bedding mortar	M4	–	–	94	–	3	–	–	4
	M21	11	2	43	8	13	19	5	–
	M35	–	3	33	16	18	29	–	2
	M36	–	–	59	15	21	–	–	6
	M37	–	3	46	14	20	5	–	12
	M39	–	7	55	–	14	12	5	7
	M40	–	5	56	14	21	–	–	4
	M41	–	5	52	13	27	–	–	3
	M43	–	53	38	–	4	–	1	5
	M44	–	28	30	9	13	11	4	5
	M45	–	–	24	22	30	16	8	–
	M46	–	–	25	13	17	12	29	5
	M49	–	46	35	–	12	–	7	–
	M50	–	52	25	8	7	–	5	3
	M52	–	4	70	9	17	–	–	–
Exterior render	M2	–	–	37	34	17	7	2	4
	M16	–	–	48	4	22	17	8	–
	M3	–	–	94	–	2	–	–	4
	M12	–	7	87	–	6	–	–	–
	M13	12	3	74	–	3	5	3	–
	M14	–	–	94	–	3	–	2	2
	M15	–	–	85	10	4	–	–	2
	M20	–	2	92	2	2	–	–	2
	M8	2	92	2	3	1	–	–	–
	M8-07	–	99	1	–	–	–	–	–
	M88-07	–	100	1	–	–	–	–	–
	M9	–	89	3	–	8	–	–	–
	M10	–	95	1	–	4	–	–	–
	M11	–	84	7	–	6	4	–	–
	M22	–	98	2	–	–	–	–	–
Surface repair	M5	–	93	1	–	6	–	–	–
	M6	–	89	2	–	8	2	–	–
	M23	–	88	1	–	6	–	–	–
	M1	–	90	8	–	2	–	–	–
	M7	–	94	2	–	4	–	–	–
	M28	6	79	3	–	6	6	–	–
	M25	3	69	11	–	16	1	–	–
	M26	4	67	7	–	15	7	–	–
	M27	9	71	7	–	10	4	–	–
Interior plasters and coatings	M29	48	–	35	–	17	–	–	–
	M30	71	10	–	–	19	–	–	–
	M31	87	–	–	–	13	–	–	–

		Gypsum	Anhidrite	Calcite	Huntite	Quartz	Feldespar	Sepiolite	Dolomite
Mortar for decoration	M24	–	13	68	15	3	–	–	2

accessorial traces of sepiolite, illite and anhydrite are also detected. Exceptionally gypsum is present as an accessory component in two samples taken from the wall of the outer courtyard, M21 as bedding mortar and M13 as external render. These samples are collected in an area of the wall that was covered by sediments but was exposed after the excavation. The chemical compositions of these mortars (Table 4) are notable for the high proportion of F, Cl and Br. The ratio Cl/Br $\sim$10 is much lower than in the other sample, which reaches values above 200. The last aesthetic render layer (*stucco render*), is mainly composed of 83–99 % of anhydrite with minor amounts of calcite (0.5–2.5 %) and occasionally traces of quartz, illite and gypsum. These samples exhibit white colour with grey hues in samples with more accessorial aggregate grains, i.e., quartz, feldspar, etc. In XRF, Sr is very high in these mortars with $CaSO_4$ as binder.

Mortars for surface repair show a fairly homogeneous mineral composition mainly composed of 70–95 % of anhydrite, with accessorial quartz (1.5–16 %), calcite (0.5–11 %) and feldspar (0–7 %). It is located both inside and outside of the tomb–chapel and the presence of gypsum (3–9 %) was only detected in the samples from the innermost rooms (central corridor and shrine). The chemical compositions of these mortars are notable for the high proportion of Sr.

Interior plasters and coating from the burial chamber also exhibit variable mineral compositions depending on their structural position. The first mortar-coating is mainly composed of gypsum (48 %) and calcite (33 %), with accessorial quartz (17 %). In contrast, the final aesthetic plaster layer consists mainly of gypsum (around 80 %) and accessorial quartz, in the absence of calcite. Also, a presence of 10 % anhydrite was detected in sample M30 (Table 3). Also worthy of mention is the mineralogical analysis of two samples (M32–33) of mortar under preparation found in a bowl on the burial chamber having great similarity to those of the first-mortar coating, gypsum 50 %, calcite 32 % and quartz 18 %.

Mortar for decoration represented by the micro-sample M24 it was collected from the white wall of Djehuty's statue niche adjoining the façade (Fig. 4d), displaying a different mineralogical approximated composition, as follows: anhydrite 13 %, calcite 68 %, huntite 15 %, quartz 2 % and dolomite 2 %. It is an interesting white and hard mortar sample including huntite as a bleaching agent and utilized as the background of Djehuty's statue.

The ESEM confirmed mineralogical and chemical analyses performed along with different categories of mortars (Fig. 5). The ESEM provided frequent images of coccolithophore fragments in carbonated mortars (Fig. 5b, c), and different calcium phosphate morphologies in the mortar aggregates (Fig. 5d, e). The backscattering probe highlights heavy elements such as zircon or REE in minerals. The cathodoluminescence probe provides spectral features of apatite grains containing REE and luminescence plots outlining their distribution. EDS analyses of zircon and monazite grains show carbon and calcium analysed into the host matrix. The monazite EDS spot analysis shows La 11.42; Ce 21.68; Nd 6.20 and Pr 1.11 % in agreement with a monazite-(Ce) standard formula (Ce, La, Nd, Th) PO_4 in our case, without Th and with Pr and Sm in similar proportions recalculating without the surrounding host calcium. We performed spectra CL from the monazite surface and several Ca-phosphate grains to observe the entrance of different proportions of REE elements in structural positions of Ca^{2+} producing characteristic narrow CL peaks associated to REE following the cathodoluminescence defect-emission attributions of Blanch [31].

Pore structure of the studied mortars also depends mainly on their use/application and mineralogical composition. All the studied mortars present very high values of porosity in which calcium sulphate mortars have higher porosity values than in calcite mortars (Table 5). Porosity values in masonry mortars for *surface repair* (50–62 %) and *calcium sulphate* exterior renders (58–68 %) are higher than *bedding mortars* (31 %) and *carbonated mortars for exterior render* (43–48 %). The pore size distribution (PSD) is poorly sorted or poly-modal, the number and volume of pore modes is defined by the binder and aggregates relationships (Fig. 6). PSD of mortars contrast with host rocks ones, which has a narrow size range. The PSD pattern is very complex, although some general tendencies can be appreciated. Calcium sulphate mortars present a mode size around 1 μm (e.g. M6, M11) whereas carbonatic mortars present a wide mode size in the 0.1–1 μm ranges (e.g. M4, M15). In sort, the amount and kind of aggregates decrease sorting.

Specific surface area values (SSA) of the studied mortars range from 1 to 18 m^2/g (Table 5). SSA values for mortars are similar to those of the host rock

Table 4 XRF analyses of mortar samples

Mortar type	Oxides (%)												
	Sample	SiO_2	Al_2O_3	Fe_2O_3 (total)	MnO	MgO	CaO	Na_2O	SO_3	K_2O	TiO_2	P_2O5	LOI
Bedding mortar	M21	30.81	7.46	4.43	0.05	2.84	28.99	0.75	0.21	0.94	0.68	0.39	22.61
Exterior render	M16	42.47	10.43	6.87	0.10	3.03	16.49	1.07	0.20	1.21	1.20	0.32	16.28
	M12	14.15	3.58	1.69	0.01	2.05	41.13	0.73	1.04	0.76	0.17	0.52	34.18
	M13	14.11	3.33	1.52	0.01	2.03	40.92	1.02	1.61	0.58	0.16	0.53	34.18
	M14	14.15	4.21	1.65	0.01	2.10	41.07	0.91	0.25	0.62	0.16	0.47	34.60
	M15	13.19	4.17	1.55	0.01	2.08	41.31	1.31	0.22	0.60	0.15	0.46	35.13
	M20	12.86	3.68	1.62	0.01	2.12	47.03	0.83	0.40	0.68	0.16	0.59	29.98
	M9	12.02	2.70	1.79	0.02	1.85	36.62	0.68	38.41	0.23	0.17	0.19	5.31
	M10	11.27	2.54	1.73	0.02	1.81	37.15	0.97	39.94	0.24	0.16	0.17	3.79
	M11	14.84	3.09	1.85	0.02	1.94	35.14	0.86	33.37	0.29	0.21	0.21	7.99
Surface repair	M25	15.70	2.30	0.93	0.09	1.92	25.34	0.25	39.36	0.14	0.11	0.18	13.32
	M27	26.47	1.67	0.87	0.02	1.68	18.35	0.31	30.39	0.23	0.13	0.13	19.20
Interior plasters and coatings	M29	11.53	1.37	0.61	0.01	1.65	41.20	0.26	23.00	0.07	0.06	0.12	20.13
	M31	7.69	1.95	1.28	0.00	2.60	28.09	0.27	35.70	0.13	0.12	0.11	21.77

Mortar type	Traces (ppm)											
	Zr	Y	Rb	Sr	Cu	Ni	Co	Ce	Ba	Cr	V	Th
Bedding mortar	105	16	13	401	12	24	10	15	184	63	74	3
Exterior render	237	26	29	448	31	47	18	51	339	116	135	11
	47	31	10	862	7	22	8	14	199	69	35	8
	58	35	11	957	10	24	8	21	161	72	35	–
	59	30	13	846	11	27	8	20	291	93	39	–
	59	28	14	817	9	26	7	18	154	93	40	–
	29	16	9	432	4	15	7	2	49	43	39	–
	–	4	–	3,983	4	12	9	21	142	33	18	–
	–	4	–	3,817	2	10	10	13	111	24	19	–
	–	2	–	2,170	3	11	7	1	84	27	20	–

Table 4 continued

Mortar type	Traces (ppm)											
	Zr	Y	Rb	Sr	Cu	Ni	Co	Ce	Ba	Cr	V	Th
Surface repair	–	4	–	3,051	8	14	8	18	301	64	26	–
	23	5	–	2,967	–	10	9	22	359	72	24	1
Interior plasters and coatings		1	–	2,273	–	7	7	13	215	37	16	–
	41	5	–	2,944	–	7	10	12	272	96	16	–

Mortar type	Traces (ppm)										
	Nb	La	Zn	Cs	Pb	Mo	F	Cl	Br	Bi	Cd
Bedding mortar	8	13	33	4	3	–	745	794	10	–	19
Exterior render	20	23	66	1	6	1	616	1,957	929	8	–
	6	17	32	10	–	–	1,006	10,350	2,409	9	–
	2	15	33	2	3	–	1,140	8,039	3,087	9	1
	4	19	38	1	2	–	1,124	2,788	1,921	12	–
	1	17	37	1	1	–	1,087	2,233	4,521	16	1
	2	8	26	4	1	–	944	6,027	1,427	14	–
	7	–	11	7	1	–	388	806	7	1	–
	10	2	10	8	1	–	581	2,111	8	1	–
	2	1	12	9	1	–	515	1,239	10	1	13
Surface repair	1	–	16	22	7	–	897	579	5	–	–
	4	11	14	13	5	–	586	484	4	–	–
Interior plasters and coatings	32	–	4	30	–	–	483	252			6
	27	3	–	28	1	–	–	210	–	–	–

(3–6 m^2/g) although they present a different PSD. The fraction of thin pores and the high porosity values for mortars explains these values. The presence of clay minerals as aggregates gives SSA values higher than the rest of the studied mortars and have special significance in M11, M14 and M21.

Table 5 Connected porosity, *P*, total porosity, P_T, and specific surface area, SSA (m^2/g), measurements of the mortar samples

Mortar type	Sample	*P* (%)	P_T (%)	SSA (m^2/g)
Bedding mortar	M4	31.30	34.63	18.34
	M21	30.89	43.73	14.37
Exterior render	M2	43.53	46.31	8.22
	M12	48.89	57.49	3.49
	M13	46.07	62.30	3.92
	M14	43.60	47.46	10.17
	M15	42.05	44.57	5.03
	M9	57.93	58.27	2.56
	M10	62.05	68.56	7.56
	M11	68.35	57.61	8.32
Surface repair	M5	62.89	61.80	9.05
	M6	55.77	56.56	7.33
	M1	55.16	53.62	1.00
	M7	51.11	52.10	1.88
	M25	57.94	62.77	1.10
	M26	50.42	–	2.36
	M27	52.77	56.64	2.10

The characterisation of mechanical strength has only been carried out for the calcium sulphate *exterior render* mortars M9, M10 and M11 due to sample size limitation. The studied mortars presented a very low compressive strength (0.25–1.60 MPa). References to the mechanical strength of ancient mortars are scarce in the literature since their determination requires large samples. Hence, we compared our results to those for repairing mortars with similar properties to the studied ancient mortars. The values obtained from micro-compressive analyses are comparable to meso-compressive values for repairing mortars [10, 30].

4 Discussion

4.1 Host rock features and construction and conservation/stability of the tomb–chapel

The host rock exhibits low mechanical strength (Table 2), relatively linear stress–strain behaviour and brittle fracture [10, 30]. The presence of a dense network of fissures intensifies its low mechanical

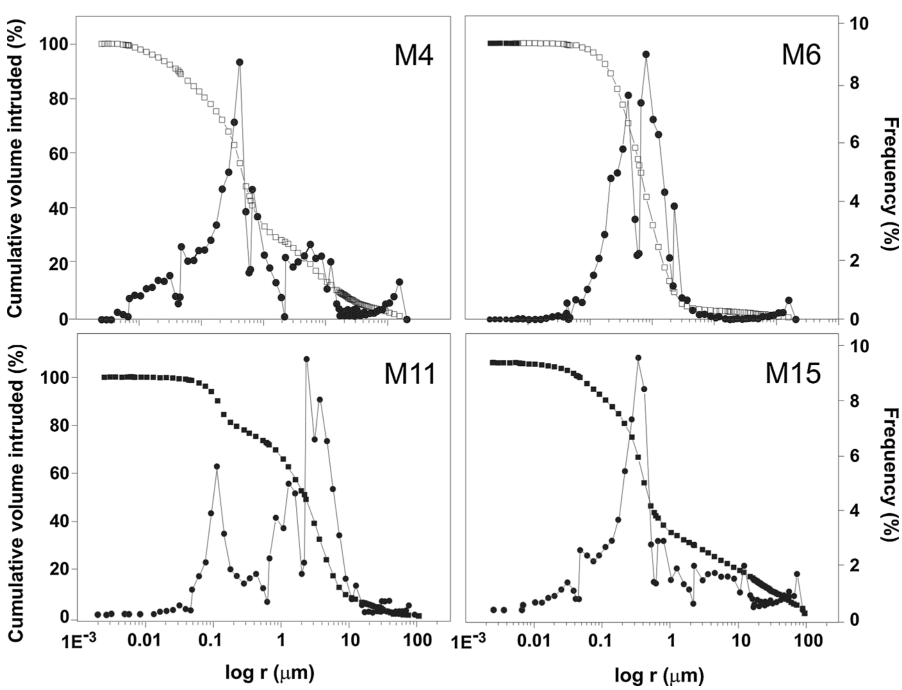

Fig. 6 Cumulative mercury intrusion and pore-size distribution curves of mortars *M*4, *M*6, *M*11 and *M*15

strength favouring an anisotropic mechanical behaviour and causing fractures, blocks dropping and subsequent collapses. The hewing of the tomb–chapel itself caused severe mechanical stress in the rock, which is confirmed by numerous boulders having fallen during the carving process, later repositioned by fixing mortars (Fig. 4c). This fact is more severe in the softer rocks of the geological sections. Compressive strength values in geological S1 and S3 are lower than in S2 and S4.

Djehuty built his tomb–chapel in the foothill of Dra Abu el-Naga, at ground level, where the limestone has the best mechanical properties of the geological column (S4). The host rock at this level is massive and stable enough to allow relief carving and then covering the surface with a very thin whitewash layer upon which the pigments could be applied. Even now some of the walls of the tomb exhibit a relatively good state of conservation and some painting remains. The burial chamber was hewn into a massive limestone level (S1) but with poorer mechanical properties (Table 2). These properties were probably considered when it was decided not to decorate it in relief, but at this level it was advisable to use mortars, preparation layers and finally the pigments. Moreover, in this geological section, salt weathering is commonly linked to capillary waters. The burial chamber reaches down to 12 m below ground level, a few meters above the Nile water table. The water table undergoes significant seasonal oscillations and still today there is a variation between summer and winter associated with dam gates opening and closing. PSD curves of host rocks are well sorted and show a pore mode in the size interval of 0.04–0.2 μm (Fig. 3). Capillary water transport is active in this pore range and the capillary forces are important [29]. This movement, although slow, periodically transports water with ions to the burial chamber's walls and after dry seasons, salt precipitation is then observed. The host rock is susceptible to weathering by salt crystallization. It presents significant values of connected porosity, small pore size (circa 0.1 μm) and low mechanical strength which favour the effectiveness of salt stress.

Gypsum and halite salts are frequently observed on surfaces particularly on the lower half of the burial chamber's walls and inside cracks of the host rock in S1 (Fig. 3). Hence, rock deterioration by salt weathering is not really significant because the crystallization pressures of gypsum and halite are relatively harmless [32, 33] and the air remains constant most of the time. Salt deterioration takes place by repeated crystallization-dissolution process prompted by variations in the RH and temperature [32]. As a result, the stable and dry microclimatic conditions of Djehuty's tomb–chapel reduce the salt deterioration in the porous materials and salts tend to grow as efflorescence (mainly gypsum and halite), causing aesthetic and physical surface damage. Limestone bedrock salts migrate to the rock–mortar interface and precipitate detaching mortar plates from the rock.

4.2 Provenance and stability of the mortars

The application of a proper combination of analytical techniques [19] on mortars has shown obvious relationships between their intrinsic properties and specific use in the tomb–chapel of Djehuty. Bedding mortars of the external masonry are the least porous (~30 %) which provide the best mechanical properties to be used as structural mortars. The suitable ratio of clay and quartz in the exterior renders ensures adequate strength and flexibility properties for these mortars. Clay acts as a binder and plastic medium to glue together with the other ingredients. The sand grains ensure stretch when dry. The inclusion of straw reduces cracking, ensures the strength and also the speed in drying. The presence of calcite improves the mechanical resistance and stability. The final calcium-sulphate stucco renders not only improve the appearance of the exterior walls, but also help to protect them against weathering and add to their mechanical strength [5]. The tomb–chapel is hewn into a brittle fossiliferous chalk which experienced collapses during the building process, and was later filled with calcium sulphate mortars for surface repairs widely utilized in the tombs. The sub-group of interior mortars used in the transversal hall and most external areas are mostly anhydrite while the most internal mortars, e.g., the innermost room or shrine, have remains of gypsum and include a larger proportion of agglomerates, i.e., calcite, quartz and feldspar grains. In these gypsum-based mortars it is common to observe euhedral crystals of celestine ($SrSO_4$) (Fig. 5f). Celestine precipitation could be related to the process of gypsification of anhydrite by the liberation of strontium and precipitation as euhedral celestine. This could indicate that the original raw material used in the manufacture of these plasters could be anhydrite from the sediments of the Esna formation. Finally, in the burial chamber the first coating of ceiling mortar displays 35 % of calcite, suggesting a possible attempt to improve the resistance of the ceiling avoiding further collapses. However, the massive use of gypsum with 20 % of quartz in the final plastering of the painted burial chamber walls could be explained by the fact that in the high RH conditions of this chamber, the lime-putty hardening is very slow. Occasionally this type of mortar and plaster application was used as substrates for decoration, rectifying the poor quality of the local limestone as a surface for carving and painting. They would be prepared on a surface of plaster upon which the pigment could be applied in *tempera* rather in *fresco secco* [5]. I.e., they ensured that the pigment adhered to the surface by use of a binding medium without remoistening the plaster surface. These painted plaster surfaces are common in tomb–chapels on the West Bank at Thebes, where it is typical to find it on walls and ceilings and sometimes in burial chambers [5].

Analyses of mortar samples could additionally provide an insight into the provenance of the materials used by the ancient Egyptian builders to manufacture the different types of mortar. Commonly carbonated mortars show coccolithophore fragments coming from the local rocks. It is difficult to clarify their role as an aggregate or as relicts of poorly burnt lime-putty under the theoretical ~850 °C necessary for the thermal decomposition of calcite. These coccoliths of eukaryote phytoplankton are important constituents of the Thebes limestone facies of the central Nile Valley, and are studied using coccolith biostratigraphy techniques [34, 35]. The mineralogical analyses (Table 3) and observation under microscopes (Fig. 5) of the aggregate bodies are in good agreement with the previously studied surrounding rocks composed of smectite, illite, kaolinite, sepiolite, calcite, dolomite, quartz, anhydrite and gypsum. With regard to the provenance of the accessorial calcium phosphate minerals found in the mortars, it seems clearly anthropogenic due to the addition of bones in the mixing of raw materials prior to firing. The Ca-phosphate firing, wetting and re-crystallization processes took place in different ways producing clean hydroxyapatite or doped with REE associated to detritus from endogenous rocks in phases such as monazites and zircons. In short, the provenance of the materials points to the nearby surrounding areas. The high proportion of Cl and Br in the carbonated mortar render seems to imply that the water used is much more concentrated in salt than that used for the rest of the mortar.

Finally, the stability of the mortars is related to micro-environmental conditions. *Lime mortars* showed high values of porosity similar to the other ancient lime mortars. The observed high porosity can be attributed to cracking after drying linked with the high binder content [36]. Porosity values for calcium sulphate mortars are particularly high (Table 5). Nowadays the mineralogical composition of binders is mainly anhydrite but initially was applied as gypsum. Over time, in hot and dry climatic conditions, gypsum slowly transforms into anhydrite. The desiccation from gypsum to anhydrite involves volume reduction and deterioration. Since the molar volume of gypsum and anhydrite are respectively 74.69 and 45.94 cm^3/mol, the dehydration reaction converts 100 % gypsum in 60 % anhydrite and 40 % porosity. In the painted burial chamber under stable high levels of RH, gypsum mortars remain preserved from dehydration and consequent cracking (M30 and M31). Previous processes of wetting–drying during episodes of rise–fall of the Nile River and especially during past openings of the chamber dissolved bedrock salts which migrated to the rock–mortar interface. Efflorescence gypsum and halite salts are frequently observed, particularly on the lower half of the burial chamber's walls, causing aesthetic and surface physical damage. The proximity of the Nile water table was favourable to the air of the burial chamber originally reaching a high RH level circa 80 %. However, once the burial chamber was excavated air RH dropped and it is currently oscillating from 40 to 65 % throughout an annual cycle. It is known that salt deterioration is carried out by repeated dissolution–crystallization process promoted by changes in the RH and temperature [32]. Maintaining stable RH conditions at this level of the tomb–chapel seems to be the most reasonable recommendation to avoid mineral phase changes—mainly gypsum desiccation and crystallization–deliquescence for halite—and hence to ensure the preservation of these mortars. Thus nowadays, the burial chamber is kept closed during the archaeological works to maintain stable environmental conditions and prevent desiccation processes.

5 Summary and conclusions

The analyses of rock and mortars from the outer courtyard and inside Djehuty's tomb–chapel provided data on the techniques used by the ancient Egyptian builders. The specific properties of the host rock and the local environment play important roles in the construction of funerary monuments and in the evolution of mortar pastes. A comprehensive knowledge of materials will make it possible to design mortars compatible with conservation in the funerary complex of Djehuty. These results showed that Djehuty built his tomb–chapel with a view to using the best mechanical properties of the geological material. Problems of instability and falling blocks of geological lower quality levels were solved by applying the appropriate mortar in each case. Furthermore, outside the tomb–chapel, several mortar types were applied for erecting masonry elements such as courtyard walls and façades. The sources of the mortar raw materials are local.

The upper level of the tomb–chapel was hewn into a massive limestone with the best mechanical properties. This level was decorated in relief, but mortars were applied onto the host rock to solve blocks that had collapsed during the building process. These mortars for surface repair are calcium sulphate based mortars, where most external areas are cleaner anhydrite while the more interior mortars (shrine) have remains of gypsum and include a higher proportion of agglomerates, i.e., calcite, quartz and feldspar grains.

The burial chamber was hewn into a limestone level with poorer mechanical properties. The instability of the host rock was solved by applying a plaster layer as a first coating, a gypsum based mortar but with a high proportion of calcite and accessorial quartz. A final aesthetic gypsum plaster layer was applied, on which the Book of the Dead was painted.

The courtyard is delimited by both rock-carved and masonry walls. The mineral composition in the masonry bedding mortars is variable depending on the different construction stages, but carbonated bedding mortars prevail. The mud–brick and rock-carved walls were covered by exterior renders. These renders are layer-structured. The first carbonated-mud mortar layer is a mixture of limestone, mud and straw fragments. The second fine-grained carbonated mortar layer is mainly composed of calcite and straw, with minor amounts of illite, quartz, dolomite and/or sepiolite. Finally, an outer aesthetic stucco layer is mainly composed of anhydrite.

The specific dry environment outside the tomb–chapel plays an important role in the evolution of the mortar pastes. The mineralogical composition of the raw material of the calcium sulphate binder was anhydrite prior to application and the original mineralogical composition of the calcium sulphate binder was gypsum when it was applied on the walls. But under the hot and dry climatic conditions, outside and in the shallower areas of the tomb, gypsum was again transformed into anhydrite over time. Currently, maintaining stable RH conditions at the upper level of the tomb–chapel seems to be the most reasonable recommendation for preserving these mortars. Furthermore, Djehuty's burial chamber is sited close to the water table of the Nile River and originally reached a high RH level circa 80 %. Natural gypsum and halite salts infiltrate on the lower half of walls. The high humidity has a positive effect in keeping the gypsum plaster layers in their original condition, preserving them from dehydration. The burial chamber is closed after each archaeological season and RH is recovered up to 65 %. It is recommendable maintaining stable this RH to avoid mineral phase changes so as to ensure preservation of the mortars. The micro-environmental conditions are critical for preserving mortars and paintings. Therefore, knowing and stabilizing the optimum environmental conditions is essential in order to ensure the preservation of such materials.

Acknowledgments The archaeological field works in Egypt were supported by the CajaMadrid Foundation (Madrid, Spain). The expedition is now sponsored by Union Fenosa Gas and the Spanish Ministry of Culture.

References

1. Manita P, Triantafillou TC (2011) Influence of the design materials on the mechanical and physical properties of repair mortars of historic buildings. Mater Struct 44:1671–1685
2. Van Balen K, Papayianni I, Van Hees R, Binda L, Waldum A (2005) Introduction to requirements for and functions and properties of repair mortars. Mater Struct 38:781–785
3. Válek J, Hughes JJ, Groot C (2012) Historic mortars: characterisation, assessment, conservation and repair, vol 7., RILEM bookseriesSpringer, Berlin, pp 1–12
4. Camuffo D (2014) Microclimate studies for cultural heritage: conservation, restoration and maintenance of indoor and outdoor monuments, 2nd edn. Elsevier, New York

5. Nicholson PT, Shaw I (2006) Ancient Egyptian materials and technology, 4th edn. Cambridge University Press, Cambridge, UK
6. Ragaï J, Poyet T, Beurroies I, Rouquerol F, Llewellyn P (2002) Characterising the porous structure of Egyptian mortars using thermoporometry, mercury intrusion porometry and gas adsorption manometry. Stud Surf Sci Catal 144:435–441
7. Lucas A (2003) Ancient Egyptian Materials and Industries, 4th edn. JR Harris, Edward Arnold, London
8. Garcia-Guinea J, Sanchez-Moral S, Correcher V, Sanchez-Muñoz L, Cuezva S, Cremades A, Benavente D, Galan JM (2008) Phosphor plasters of CaSO4: Dy on the courtyard wall of Djehuty's tomb (Luxor, Egypt). Radiat Meas 43:849–853
9. Mahmoud H (2009) Examination of some inorganic pigments and plaster layers from excavations at Saqqara Area, Egypt: optical microscopy and SEM-EDS microanalysis. E-Conserv Mag 12:38–46
10. Sanchez-Moral S, Martinez-Martinez J, Benavente D, Cuezva S, Fernandez-Cortes A (2011) Mechanical characterization of ancient Egyptian mortars. Key Eng Mater 465:487–490
11. Pinińska J, Attia HR (2003) Use of geomechanical research in the conservation of stone monuments (Maadi Town Temple, Fayoum, Egypt). Geol Quart 47:1–12
12. Hemeda S (2013) Geomechanical investigations for architectural heritage preservation, the Habib Sakakini palace in Cairo, Egypt. Int J Conserv Sci 4:43–52
13. Moussa AMA, Kantiranis N, Voudouris KS, Stratis JA, Ali MF, Christaras V (2009) The impact of soluble salts on the deterioration of Pharaonic and Coptic wall paintings at Al Qrna, Egypt: mineralogy and chemistry. Archaeometry 51:292–308
14. Moussa AB, Kantiranis N, Voudouris KS, Stratis JA, Ali MF, Christaras V (2009) Diagnosis of weathered Coptic wall paintings in the Wadi El Natrun region. Egypt J Cult Herit 10:152–157
15. Maekawa S (1993) Environmental monitoring at the Tomb of Nefertari. In: Corzo MA, Afshar M (eds) Art and eternity: the Nefertari wall paintings conservation project, 1986–1992. Getty, Los Angeles, CA
16. Papayianni I, Pachta V, Stefanidou M (2013) Analysis of ancient mortars and design of compatible repair mortars: the case study of Odeion of the archaeological site of Dion. Constr Build Mater 40:84–92
17. Bartz W, Rogó J, Rogal R, Cupa A, Szroeder P (2012) Characterization of historical lime plasters by combined non-destructive and destructive tests: the case of the sgraffito in Bonów (SW Poland). Constr Build Mater 30:439–446
18. Rossi-Doria PR (1990) Report on the RILEM Workshop "Ancient mortars and mortars for restoration" taken place in Ravello (Italy), 9–11 November, 1988. Mater Struct 23:235–238
19. Groot C, Ashall G, Hughes JJ (2004) Characterization of old mortars with respect to their repair. Final report of RILEM TC 167-COM. RILEM Publications SARL, Bagneux, France
20. Hughes JJ (2012) RILEM TC 203-RMH: repair mortars for historic masonry. The role of mortar in masonry: an introduction to requirements for the design of repair mortars. Mater Struct 45:1287–1294
21. Moropoulou A, Bakolas A, Anagnostopoulou S (2005) Composite materials in ancient structures. Cem Concr Compos 27:295–300
22. Galan JM (2009) Early Investigations in the tomb–chapel of Djehuty (TT 11). In: Magee D, Bourriau J, Quirke S (eds) Sitting beside Lepsius: studies in honour of Jaromir Malek at the Griffith Institute. OLA 185:155–181
23. Galán JM (2013) The book of the dead in the burial chamber of Djehuty (TT 11). Egypt Archaeol 42:21–24
24. Said R (1990) The geology of Egypt. A.A. Balkema, Rotterdam
25. Tawfik HA, Zahran EK, Abdel-Hameed AT, Maejima W (2011) Mineralogy, petrography, and biostratigraphy of the Lower Eocene succession at Gebel El-Qurn, West Luxor, Southern Egypt. Arab J Geosci 4:517–534
26. Shaaban MN (2004) Diagenesis of the lower Eocene Thebes formation Gebel Rewagen area, Eastern Desert, Egypt. Sedim Geol 165:53–65
27. Wüst RAJ, McLane J (2000) Rock derioration in the royal tomb of Seti I valley of the Kings, Luxor, Egypt. Eng Geol 58:163–190
28. National Climatic Data Center/NESDIS/NOAA/U.S. (2003): U.S.A.F. DATSAV3 Surface Observations, 1901-continuing. Research data archive at the National Center for Atmospheric Research, Computational and Information Systems Laboratory. http://rda.ucar.edu/datasets/ds463.2/
29. Benavente D, Cultrone G, Gomez-Heras M (2008) The combined influence of mineralogy, hydric and thermal properties in the durability of porous building stones. Eur J Min 20:673–685
30. Nakhla SM, Abd El Kader M (2006) Mortars and stones for the restoration of masonry works in the Sphinx. In: Daoud K, Abd el-Fatah S, editors. The world of ancient Egypt. Essays in Honor of Ahmed Abd el-Qader el-Sawi. Supplément aux Annales du Service des Antiquités de l'Egypte, Cahier no, 35. pp 207–215
31. Blanc P, Baumer A, Cesbron F, Ohnenstetter D, Panczer G, Remond G (2000) Systematic cathodoluminescence spectral analysis of synthetic doped minerals: anhydrite, apatite, calcite, fluorite, scheelite and zircon. In: Pagel M, Barbin V, Blanc P, Ohnenstetter D (eds) Cathodoluminescence in geosciences. Springer, Berlin, pp 127–160
32. Benavente D, Sanchez-Moral S, Cortes-Fernandez A, Cañaveras JC, Elez J, Saiz-Jimenez C (2011) Salt damage and microclimate in the Postumius Tomb, Roman Necropolis of Carmona, Spain. Environ Earth Sci 63:1529–1543
33. Charola AE, Pühringer J, Steiger M (2007) Gypsum: a review of its role in the deterioration of building materials. Environ Geol 52:207–220
34. Tantawy AAAM (2006) Calcareous nannofossils of the Paleocene–Eocene transition at Qena region, central Nile Valley, Egypt. Micropaleontol 52:193–222
35. Aubry MP, Salem R (2012) The Dababiya Core: a window into Paleocene to early Eocene depositional history in Egypt based on coccolith. Stratigr 9:287–346
36. Sanchez-Moral S, Luque L, Cañaveras JC, Soler V, Garcia-Guinea J, Aparicio A (2005) Lime–pozzolana mortars in Roman catacombs: composition, structures and restoration. Cem Concr Res 35:1555–1565